Journal of Hazardous Materials 177 (2010) 719–729

Contents lists available at ScienceDirect

Journal of Hazardous Materials

journal homepage: www.elsevier.com/locate/jhazmat

Fluoride removal from water using activated and MnO_2-coated Tamarind Fruit (*Tamarindus indica*) shell: Batch and column studies

V. Sivasankar[a,*], T. Ramachandramoorthy[b], A. Chandramohan[c]

[a] Department of Chemistry, Thiagarajar College of Engineering (Autonomous), Madurai 625015, India
[b] PG & Research Department of Chemistry, Bishop Heber College (Autonomous), Tiruchirappalli 620017, India
[c] PG & Research Department of Environmental Sciences, Bishop Heber College (Autonomous), Tiruchirappalli 620017, India

ARTICLE INFO

Article history:
Received 27 August 2009
Received in revised form
18 December 2009
Accepted 21 December 2009
Available online 4 January 2010

Keywords:
Defluoridation
Activated Tamarind Fruit Shell
Manganese oxide-coated Tamarind Fruit Shell
FTIR
SEM
XRD

ABSTRACT

The present work is concerned with the defluoridation capacities of activated (ATFS) and MnO_2-coated Tamarind Fruit Shell (MTFS), using batch and column sorption techniques. In the batch technique, the dynamics of fluoride sorption, with respect to pH, $[F]_o$ and sorbent dose, was studied. The applicability of pseudo-first order for ATFS and Ritchie-second order for MTFS was observed. The kinetics data were found to fit well with Temkin isotherm for ATFS and Langmuir for MTFS. The interaction of co-ions in the defluoridation capacity of the sorbent was studied. Column experiments were carried out under a constant fluoride concentration of 2 mg/l, flow rate and different bed depths. The capacities of the breakthrough and exhaustion points increased with increase in the bed depth for ATFS unlike MTFS. The Thomson model was applied to the column experimental results. The characterization of the sorbents, ATFS and MTFS, was done using the FTIR, SEM and XRD techniques.

1. Introduction

Fluoride in drinking water may be beneficial or harmful to health, depending on its concentration. The optimum fluoride level in drinking water for general good health set by WHO, is considered to be between 0.5 and 1.0 mg/l. A concentration higher than this can lead to fluorosis. Fluorosis, a serious health problem for the people, is caused by an excess ingestion of fluoride. It affects the teeth and the bones and its accumulation for a long period of time can alter the DNA structure [1,2]. Several methods like adsorption [3,4], Precipitation [5], ion-exchange [6], electro-dialysis [7,8] and electro-chemical methods [9], were developed to remove the fluoride from water. In recent years, many efforts were made and, as a result more cost-effective F^- sorbents like fly ash [5], silica gel [10], bone char [11], spent catalyst [12] and zeolites [13] were developed. Among the existing techniques, adsorption is regarded as an important cost-effective technique in the developing countries where the impact of this issue is maximum. This technique is most widely used for the removal of excess fluoride from the aqueous solution. The successful and cost-effective removal of contaminants from wastewater, by adsorption techniques, demands the optimal operation of the adsorption units. To optimize the study, the design parameters must be obtained through adsorption equilibrium and kinetic results. After the equilibrium data are generated through a simple batch experimental set up, it is common practice to validate the various isotherm models to choose a model (or models) that gives the best experimental results. Popuri et al. [14] studied the biosorption of chromium(VI) using Tamarind (*Tamarindus indica*) Fruit Shell and suggested it as a good sorbent. Similarly, Bhargava and Sheldarkar [15] attempted the sorption of phosphate onto unrinsed and rinsed-tamarind-nutshell-activated-carbons and the sorption kinetics was found to fit with the pseudo-second order and Elovich models with high correlation coefficient values. Sriramachari [16] and Maruthamuthu and Venkatanarayanareddy [17] reported the binding of fluoride by tamarind *in vitro*. Huang and Huang [18] stated that the pre-treatment of biomass removes the surface impurities on the biosorbents and exposes the available binding sites for sorption [19]. Venkata Mohan et al. [20] discussed the results pertaining to the adsorptive studies of fluoride onto algal biosorbent (*Spirogyra* IO2). Kemer et al. [21] have reported the removal of fluoride by waste mud from copper mine industry and Karthikeyan et al. [22] have discussed the fluoride removal from aqueous solution by conducting polypyrrole. Onyango et al. [23] achieved the removal of fluoride using surface-tailored zeolite in a fixed bed column. Fluoride removal was also reported using spray coating of adsorbent with polymer latex on sand particles

* Corresponding author. Tel.: +91 452 2482240 41; fax: +91 452 2483427.
E-mail address: vsivasankar@tce.edu (V. Sivasankar).

0304-3894/$ – see front matter © 2009 Elsevier B.V. All rights reserved.
doi:10.1016/j.jhazmat.2009.12.091

Nomenclature

q_t	amount of adsorbate sorbed on the adsorbent at time t (mg/g)
q_e	amount of adsorbate removed from aqueous solution at equilibrium (mg/g)
k_{ad}	equilibrium constant of pseudo-first order sorption (min^{-1})
k	Ritchie-second order rate constant
α	initial adsorption rate (mg/g/min)
β	desorption constant (g/mg)
k_{id}	intraparticle diffusion rate constant ($mg/g/min^{1/2}$)
C	thickness of the boundary layer
Qe	equilibrium adsorption capacity (mg/g)
Q°	monolayer surface coverage (mg/g)
b	equilibrium adsorption constant (l/mg)
K_F and n	Freundlich constants
R_L	dimensionless separation factor
q_B	capacity at the breakthrough point (mg/g)
V_B	volume of the solution passed through breakthrough point (l)
q_E	capacity at the exhaustion point (mg/g)
m	mass of the adsorbent (g)
H	bed depth (cm)
f	symmetry of the breakthrough curve
γ	linear flow rate (cm^3/cm^2 min)
h_z	mass transfer zone
k_T	rate constant (l/mg/min)
q_T	total sorption capacity (mg/g)
θ	flow rate (ml/min)

by Wu et al. [24]. In the very recent years, fluoride removal was attempted using various adsorbents like hydrated cement [25], brick powder [26], magnetic-chitosan particle [27], magnesium oxide [28] and calcined Mg–Al–CO_3 layered double hydroxides [29]. The present study has been attempted to evaluate the defluoridation potential of Activated Tamarind Fruit Shell (ATFS) and manganese oxide-coated Tamarind Fruit Shell (MTFS). The sorption process was conducted by the batch and continuous mode column techniques. Attempts have also been made to understand the sorption kinetics and mechanism of sorption. The experimental results of MTFS were compared with those of ATFS, which was the base material for the MTFS preparation.

2. Materials and methods

Raw tamarind fruit shell was collected from a local village of Tiruchirappalli District and washed with distilled water and, dried and the pre-treatment was carried out as follows. All other chemicals used in the present study were of analytical grade purchased from E-Merck India Ltd., Mumbai, India.

2.1. Sorbent

2.1.1. Pre-treatment of Tamarind Fruit Shell (TFS)

The waste tamarind fruit shell was initially washed with 0.01N HCl followed by 0.01N NaOH. Then the sorbent was washed thoroughly using distilled water and dried by exposing it to sunlight. The dried TFS was sieved for 600 μm in size.

2.1.2. Characterization of Tamarind Fruit Shell (TFS)

The pretreated TFS was characterized for moisture (%), ash (%), pH and matter soluble in water and acid.

2.1.3. Preparation of activated Tamarind Fruit Shell (ATFS)

About 30 g of TFS of 600 μm was soaked in 600 ml of 1% $CaCl_2$ solution, for 24 h. Then the soaked TFS was washed with distilled water and dried at 110 ± 5° C in an air oven for 2 h.

2.1.4. Preparation of MnO_2-coated Tamarind Fruit Shell (MTFS)

About 27 g of $KMnO_4$ was dissolved in 21 ml of distilled water in a beaker and kept in a water bath at 90 °C for 15 min. To this, 24 g of TFS was added and the suspension was mixed gently and heated in a water bath for 10 min. Then 300 ml of 2 M HCl was added to the suspension and mixed thoroughly, followed by water bath-heating for 30 min. After the completion of the reaction, the solid was cooled and washed with distilled water and 0.05 M perchloric acid until the run-off was clear.

2.2. Sorption studies

Sorption studies of fluoride were carried out by batch and column techniques. The batch equilibration method was carried out in such a way that 1 g of ATFS and MTFS was fixed as the optimum dosage for various initial fluoride concentrations, with a solution volume of 50 ml. The contents were shaken thoroughly using a shaker, rotating at a speed of 125 rpm at room temperature (30 ± 2 °C). Then the solution was filtered and the fluoride ion concentration was measured. In addition to the defluoridation capacities, the influence of variables like contact time for maximum defluoridation, dosage, pH of the medium and co-anions were also investigated. The sorption of fluoride ions on ATFS and MTFS was also studied at different initial concentrations (2–5 mg/l).

The column technique was performed using a glass column of 0.5 mm diameter and of 250 mm of length. The operation was done by the continuous flow technique and the defluoridation study was carried out with a fluoride solution of 2 mg/l for various bed depths of 6, 9, 12 and 15 cm.

2.3. Characterization of ATFS and MTFS

The surface morphology of ATFS and MTFS before and after the treatment with fluoride was visualized by SEM with the JEOL JSM 5610 microscope. The possible morphological changes may be examined using this technique for ATFS and MTFS, before and after the treatment process. The powdered diffractorgrams of the samples were obtained using the Phillips X'Pert PRO diffractometer (PANalytical make) coupled to a copper-anode X-ray tube. The FTIR patterns were recorded using the JASCO-460 plus model at ambient conditions, using KBr as diluent to determine the functional groups on the sorbents.

2.4. Methods of analysis

The fluoride determination was done by the SPADNS [30] photometric method, at 570 nm using the UV–vis spectrophotometer (UV–vis-8500, Techcomp Ltd, Hong Kong). The pH measurements were done with the pH meter of the LI613 Elico model.

Computations were made using the Microcal Origin (Version 6.0) software. The fitness of models was discussed using regression correlation coefficients (r^2).

3. Results and discussion

3.1. Characterization of ATFS

The physico-chemical characterization of ATFS was carried out. The moisture, ash, soluble matter in water and soluble matter in acid were found to be 7.55%, 74.04%, 3.9% and 10.9%, respectively.

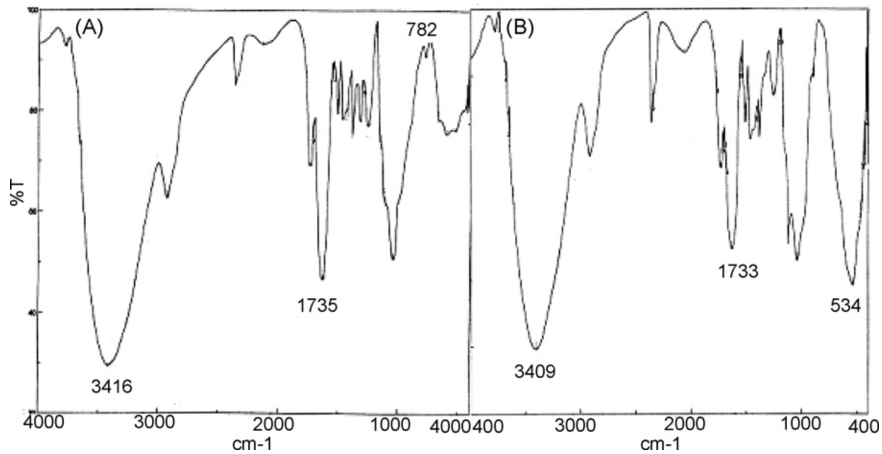

Fig. 1. FTIR spectra of (A) ATFS and (B) MTFS.

The pH of ATFS was recorded with 6.3 ± 0.3. The pore volume, density and porosity were reported to be 0.2053 cm^3, 4.869 g/cm^3 and 30.85%, respectively [14].

In order to characterize ATFS/MTFS, the FTIR, XRD and SEM analyses were carried out. The FTIR spectra (Fig. 1) show that the peaks at 3416 and 3409 cm^{-1}, are associated to the stretching frequency of –OH or–NH_2 groups for ATFS and MTFS, respectively. The peaks at 1735 and 1733 cm^{-1} exhibit the stretching frequency of >C=O group of an aromatic ester for ATFS and MTFS, respectively. An assignment at 782 cm^{-1} for ATFS, due to the presence of aromatic ortho disubstituted heterocyclic molecules, is not observed for MTFS. This indicates that there is a possibility of ring cleavage after the coating of MnO_2. An intense peak at 534 cm^{-1} indicates the stretching of Mn–O bond for MTFS. A similar work was carried out by Popuri et al. [14] for chromium sorption.

Scanning electron micrographs (Fig. 2) have depicted the sorption of fluoride onto the sorbent after the defluoridation process. SEM images are observed to be irregular clumps and the surface morphological change before and after the defluoridation process confirms the sorption of fluoride onto ATFS and MTFS. The energy-dispersive analysis of X-rays was used to analyze the elemental constituents of ATFS and MTFS. Figs. 3 and 4 represent the presence of fluoride in small amounts in the spectrum along with the principal elements C and O and minor elements like Mn. The Mn peak is observed due to the coating of manganese dioxide on ATFS. Presence of a minor peak for fluoride in Figs. 3 and 4 indicate that fluoride is superficially adsorbed on the surface of ATFS and MTFS.

Fig. 5 shows the XRD pattern of ATFS and MTFS sorbents. The material is poorly crystalline with some broad peaks especially between 20° and 25°. Similarly Shihabudeen et al. [31] and Eskandarpour et al. [32] observed the poorly crystalline nature of the sorbents in their study for the removal of fluoride in aqueous solution.

3.2. Effect of contact time

In the batch studies, it was observed that a maximum concentration of fluoride removal was attained within 30 min and thereafter, it almost remained static for both ATFS and MTFS. The period of contact time of 30 min for further studies was fixed. The fluoride removal capacity was 1990 mg F^-/kg of both ATFS and MTFS at a pH value of 6.5.

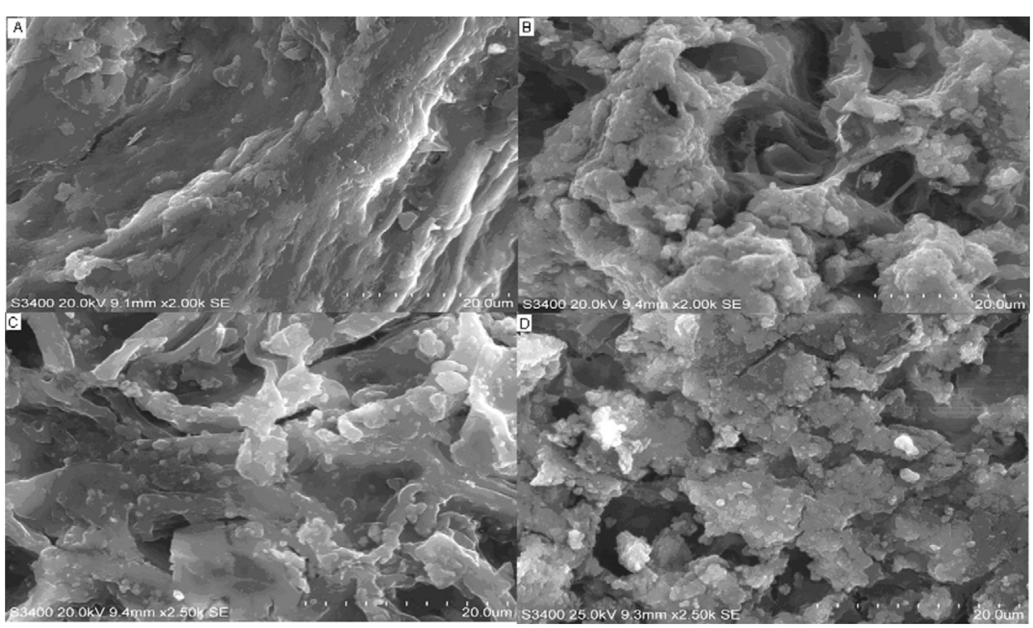

Fig. 2. Scanning Electron Micrograph (A) ATFS before fluoride sorption, (B) ATFS after fluoride sorption, (C) MTFS before fluoride sorption and (D) MTFS after fluoride sorption.

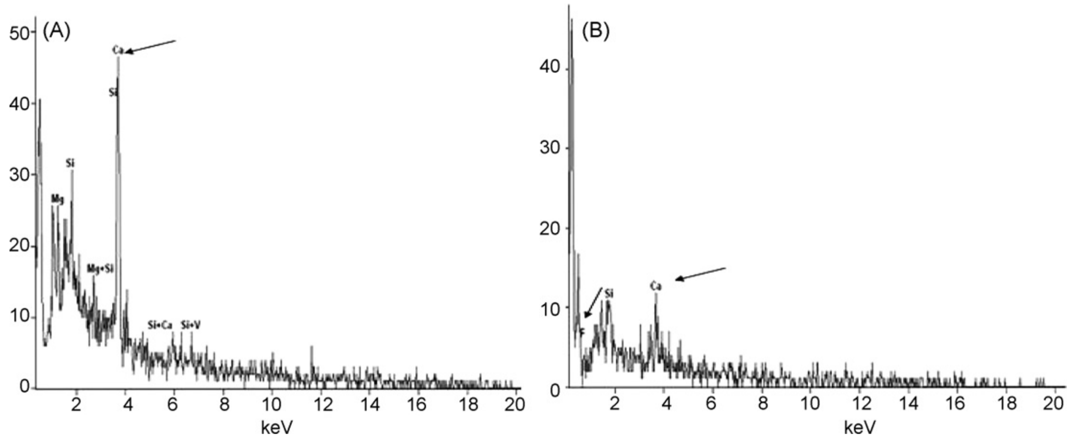

Fig. 3. EDAX for ATFS (A) before fluoride sorption and (B) after fluoride sorption.

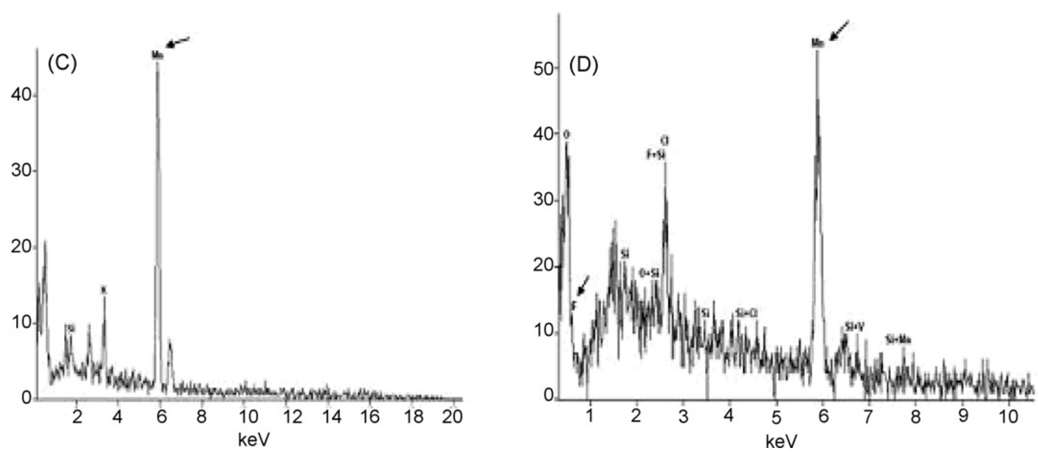

Fig. 4. EDAX for MTFS (C) before fluoride sorption and (D) after fluoride sorption.

3.3. *Effect of dosage*

In order to fix the minimum dosage for maximum fluoride removal, experiments, as a function of dosage, were carried out. The percentage removal of fluoride for both ATFS and MTFS at different dosages (0.2–1.0 g) was measured. It was observed as shown in Fig. 6B that the percentage removal increased with respect to the increased dosage and then remained constant after 0.8 g of both ATFS and MTFS. Hence the sorbent dosage was optimized to be 1 g for further experimental studies. The increase in sorption capacity with increase in dosage is apparent, because any adsorption process depends upon the number of active sites. The above justification holds good for both ATFS and MTFS.

3.4. *Effect of pH*

The removal of fluoride ions from aqueous fluoride solution was highly dependent on the solution pH in many cases, as it altered

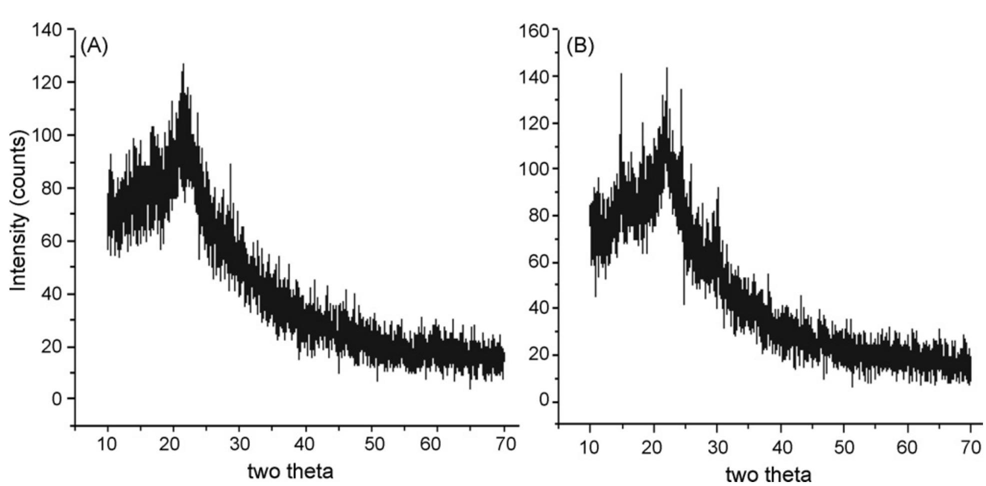

Fig. 5. XRD pattern of (A) ATFS and (B) MTFS.

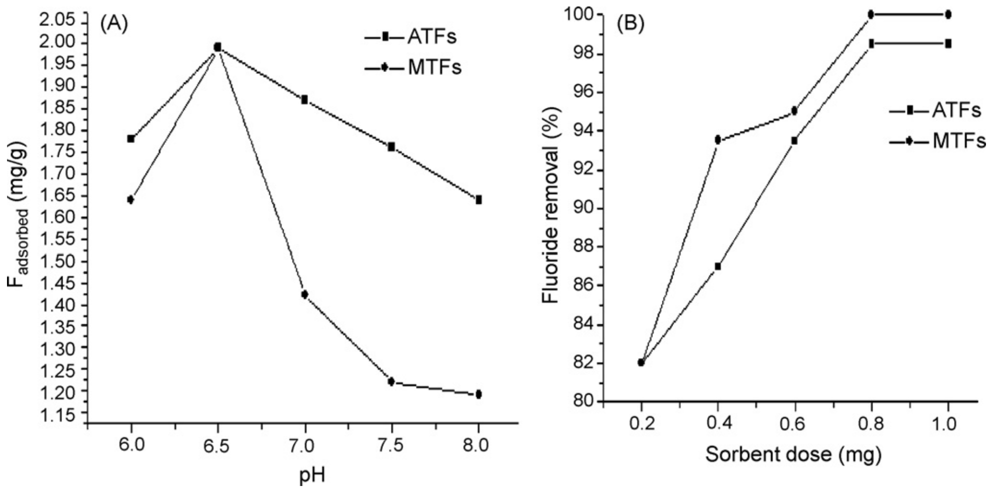

Fig. 6. Influence of (A) pH and (B) dosage of adsorbent on Fluoride sorption for ATFS and MTFS.

the surface charge on the sorbents [33]. Tamarind shells are a rich source of protein and amino acids [34]. Some functional groups, such as amines, are positively charged when protonated and may electro-statistically bind with negatively charged species. At a pH value of 6.5, for both ATFS and MTFS, the maximum removal efficiency was observed at the initial value of 6.5 (Fig. 6A). However, above the pH of 6.5, the removal was slightly reduced for ATFS, but the removal was greater for MTFS than ATFS. The increase in the pH value decreases the sorption of fluoride, as the deprotonation on the sorbent commences. This results in decreasing the electrostatic force of attraction between the sorbent and sorbate ions. A sharp decrease in fluoride removal may be due to the formation of the weakly ionised HF ($pK_a = 3.2$) at low pH values and due to the competitiveness of the OH^- and F^- ions in the bulk, at high pH values [35]. To understand the fluoride sorption behaviour under different pH values, the following reactions are considered [36,37]:

$$HF \leftrightarrow H^+ + F^-$$

$$\equiv SOH + H^+ \leftrightarrow \equiv SOH_2{}^+$$

$$\equiv SOH + OH^- \leftrightarrow \equiv SO^- + H_2O$$

$$\equiv SOH_2{}^+ + F^- \leftrightarrow \equiv SF + H_2O$$

$$\equiv SOH + F^- \leftrightarrow \equiv SF + OH^-$$

where $\equiv$SOH, $\equiv SOH_2{}^+$ and $\equiv SO^-$ are the neutral, protonated and deprotonated sites on ATFS and MTFS and $\equiv$SF is the active site–fluoride complex (S = ATFS/MTFS).

3.5. Effect of co-ions: binary component system

In this study, the individual effects of co-existing ions, which include $CO_3{}^{2-}$, $HCO_3{}^-$, $SO_4{}^{2-}$, Cl^- and $NO_3{}^-$, usually present in the groundwater samples, have been investigated through batch studies. The initial concentration of fluoride was maintained as 2 mg/l. The initial pH was maintained at 6.5 ± 0.2. Though both ATFS and MTFS follow the same trend, ATFS has greater fluoride removal efficiency than MTFS. Our experimental results revealed that there was a significant influence on the fluoride removal capacity for both ATFS and MTFS. The influence of the co-ions on the defluoridation capacity is depicted in Fig. 7A and B, which show that the fluoride sorption due to $HCO_3{}^-$ (140 mg/l) was decreased by 63.5% for ATFS whereas it decreased by 98% for MTFS. A similar interfering role on the fluoride removal was earlier reported in the defluoridation property of MnO_2-coated activated alumina [38]. This may be attributed to the competition of bicarbonate ions with the fluoride ions at the active site, on the surface of the sorbents. The selective nature of the fluoride by the sorbent depends on size, charge, polarizability, electronegativity difference, etc. The preference of the sorption of anions by ATFS and MTFS may be in the following order, $F > HCO_3{}^- > CO_3{}^{2-} > SO_4{}^{2-} > Cl^- > NO_3{}^-$.

4. Sorption dynamics

To understand the sorption mechanism, such as mass transfer and chemical reaction processes, two types of models, viz., reaction-based and diffusion-based models, were applied, to test the fitness of the experimental data. Table 1 represents the values of the constants of the kinetic models like pseudo-first order, Ritchie-second order and Elovich, for the sorption of fluoride on ATFS and MTFS.

In order to investigate the sorption mechanism of fluoride removal, pseudo-first order and Ritchie-second order kinetic models have been used at different experimental conditions.

4.1. Pseudo-first order model

A simple pseudo-first order kinetic model [39] is represented as:

$$\log(q_e - q_t) = \frac{\log q_e - k_{ad}}{2.303(t)} \qquad (1)$$

where q_t (mg/g) is the amount of fluoride sorbed on the surface of the sorbents ATFS and MTFS at time t, and k_{ad} is the equilibrium rate constant of pseudo-first order sorption (min^{-1}). The straight line plots of $\log(q_e - q_t)$ against t for different experimental conditions will give the value of rate constants (k_{ad}). The linear plots of $\log(q_e - q_t)$ against t give straight line which indicates the applicability of the Lagergren equation(Fig. 8A and B). The values of k_{ad} and the correlation coefficient (r^2) computed from these plots are given in Table 1. The pseudo-first order model (Eq. (1)) seems to be viable for both ATFS and MTFS.

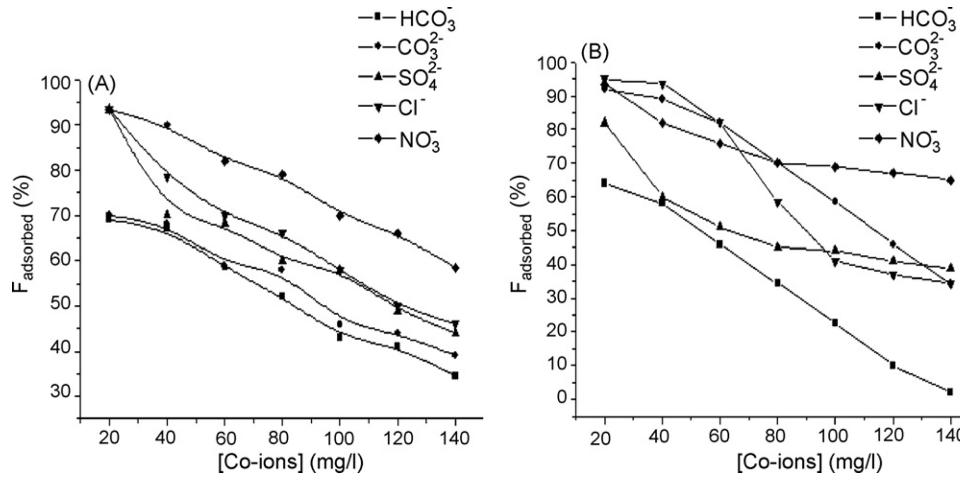

Fig. 7. Interference of co-ions in F sorption by (A) ATFS and (B) MTFS.

4.2. Ritchie-second order model

In addition, the Ritchie-second order model [40] is also used. The kinetic model can be expressed as

$$\frac{q_e}{q_e - q_t} = 1 + k_2 t \quad (2)$$

where q_t and q_e (mg/g) are the amounts of fluoride sorbed on the surface of ATFS and MTFS at any time, t and at equilibrium, k is the Ritchie-second order rate constant is obtained from the slope of the linear plots of $q_e/q_e - q_t$ against t, for different experimental conditions. The plot of q_e/q_t versus t, gives a straight line with high correlation coefficient r^2 values, which indicate the applicability of the Ritchie-second order model (Eq. (2)) whose data are shown in Table 1.

4.3. Elovich model

The Elovich equation [41] is generally expressed as follows:

$$\frac{Dqt}{dt} = \alpha \exp(-\beta q_t) \quad (3)$$

where q_t is the sorption capacity at time t (mg/g), α is the initial sorption rate (mg/g/min) and β is the desorption constant (g/mg) during any one experiment.

To simplify the Elovich equation, Chien and Clayton [42] assumed $\alpha\beta \gg 1$, and by applying the boundary conditions $q_t = 0$ at time $t = 0$ and $q_t = q_t$ at $t = t$, Eq. (3) becomes [43]:

$$q_t = \beta \ln(\alpha\beta) + \ln(t)$$

Thus, the constants can be obtained from the slope and the intercept of a straight line plot of q_t against $\ln t$. A high positive correlation may be an indication of fluoride sorption on ATFS and MTFS and the obtained b values approve the ability of sorbents to hold the fluoride ions through chemisorption (Fig. 9A and B).

4.4. Intraparticle diffusion model

In this model [44,45], the adsorbate moves from the solution phase to the surface of the adsorbent particles, in several steps. The overall adsorption process may be controlled by one or more steps (e.g., film or external diffusion, pore diffusion surface diffusion and adsorption on the pore surface, or a combination or more than one step). In a rapidly stirred batch process of adsorption,

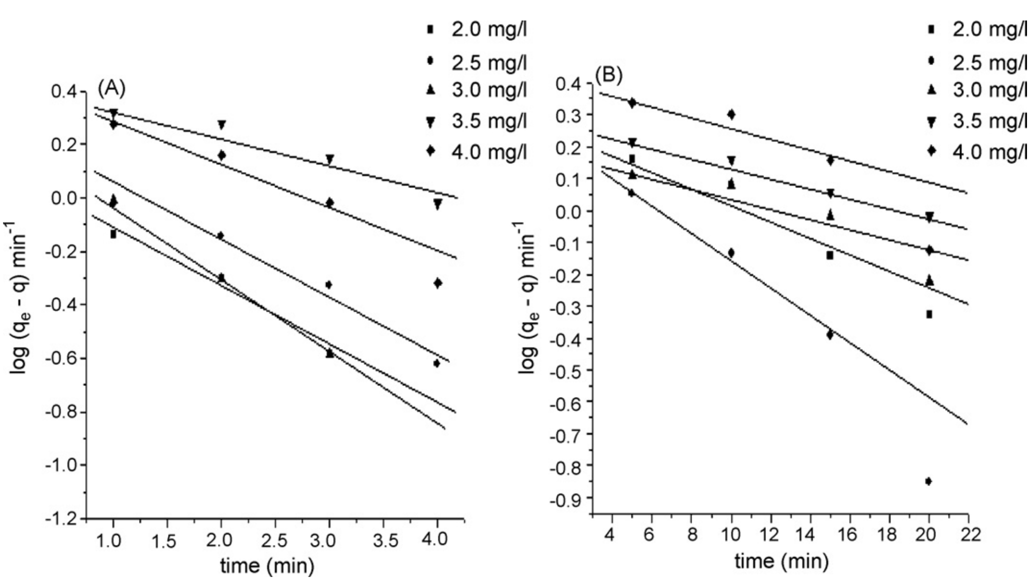

Fig. 8. Pseudo-first order kinetic model for (A) ATFS and (B) MTFS at various fluoride concentrations.

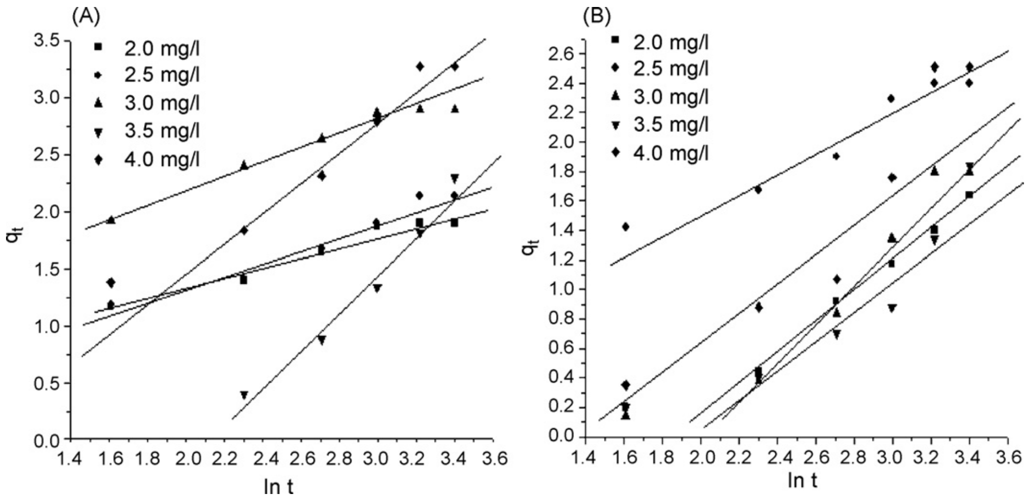

Fig. 9. Elovich model for (A) ATFS and (B) MTFS for various fluoride concentrations.

the diffusive mass transfer can be related by an obvious diffusion coefficient, which will fit experimental adsorption rate data. Normally, a process is diffusion-controlled if its rate is dependent on the rate at which components diffuse toward each other. The possibility of intraparticle diffusion was explored using the intraparticle diffusion model:

$$q_t = k_{id}t^{1/2} + C \quad (4)$$

where k_{id} is the intraparticle (pore) diffusion rate constant (mg/g/time$^{1/2}$) and C is the intercept that gives an idea about the thickness of the boundary layer. The larger the value of C, the greater the boundary-layer effect. Fig. 10A and B shows a plot of the mass of fluoride adsorbed per unit mass of ATFS and MTFS (q_t as mg/g) versus the square root of contact time ($t^{1/2}$ as min$^{1/2}$). Seemingly, the data points in Fig. 10A and B, could be connected by two straight lines: the first linear portion for macropore diffusion and the second depicting micropore diffusion. The extrapolation of the first linear portion of the plots should not pass through the origin, as the adsorption rate of fluoride onto the ATFS and MTFS, was not solely controlled by pore diffusion. If the data points shown in Fig. 10A and B were to be connected by zero, the initial sharp line showing the variation of q_t versus $t^{1/2}$ should be attributed to the boundary-layer diffusion effect or an external mass transfer effect [46,47]. The increase of k_{id} with respect to the increase in concentration indicates the higher pore sorption possibility of fluoride onto ATFS and MTFS at room temperature. Therefore, the adsorption of fluoride onto ATFS and MTFS was governed by the combined effects of surface and intraparticle diffusion. The present observation is consistent with the reported works [48].

Table 1
Kinetic models for UCTS and MCTS at various fluoride concentrations.

Pseudo-first order model						
$[F]_o$	UCTS			MCTS		
	k_1	q_e	R^2	k_1	q_e	R^2
2.0	3.35	1.60	0.9721	9.34	1.43	0.9352
2.5	5.95	1.24	0.9575	3.96	1.50	0.9634
3.0	2.19	1.83	0.9161	7.32	1.29	0.9541
3.5	1.6	1.61	0.9895	2.29	1.36	0.9415
4.0	2.88	1.68	0.9270	3.94	1.70	0.9585
Intraparticle diffusion model						
	k_i	C	R^2	k_i	C	R^2
2.0	0.25	0.65	0.9416	0.43	0.79	0.9800
2.5	0.32	0.45	0.9809	0.34	0.65	0.9576
3.0	0.31	1.36	0.9106	0.58	1.29	0.9592
3.5	0.66	1.52	0.9513	0.48	1.06	0.9125
4.0	0.64	0.10	0.9794	0.79	1.75	0.9129
Elovich model						
	a	b	R^2	a	b	R^2
2.0	0.42	0.45	0.9630	1.25	0.82	0.9569
2.5	0.19	0.57	0.9599	0.37	0.61	0.9474
3.0	1.04	0.58	0.9663	1.73	1.03	0.9177
3.5	3.64	1.70	0.9735	1.36	0.83	0.9206
4.0	0.54	1.12	0.9674	1.85	1.23	0.9168
Ritchie model						
	K		R^2	k		R^2
2.0	0.47		0.9256	0.25		0.9149
2.5	0.44		0.9267	0.24		0.9734
3.0	0.93		0.9813	0.12		0.9104
3.5	0.09		0.9307	0.05		0.9797
4.0	0.34		0.9308	0.18		0.9208

5. Adsorption isotherm analysis

The equilibrium data for fluoride sorption onto ATFS and MTFS at pH 6.5 ± 0.2 are shown in Table 2. The equilibrium data have been analyzed by the linear regression of isotherm model equations, viz., Langmuir, Freundlich and Temkin.

Table 2
Adsorption isotherms.

Isothermal models	Parameters	UCTS	MCTS
Freundlich	r^2	0.9212	0.9396
	n	4.3048	2.4073
	$1/n$	0.2323	0.4154
	K_F	1.7073	2.6946
Langmuir	r^2	0.9538	0.9643
	Q°	0.2145	0.2178
	b	148.5	40.3
	R_L	0.0036	0.0122
Temkin	r^2	0.9653	0.9265
	B_1	0.5473	0.3154
	k_T	293.6	429.0

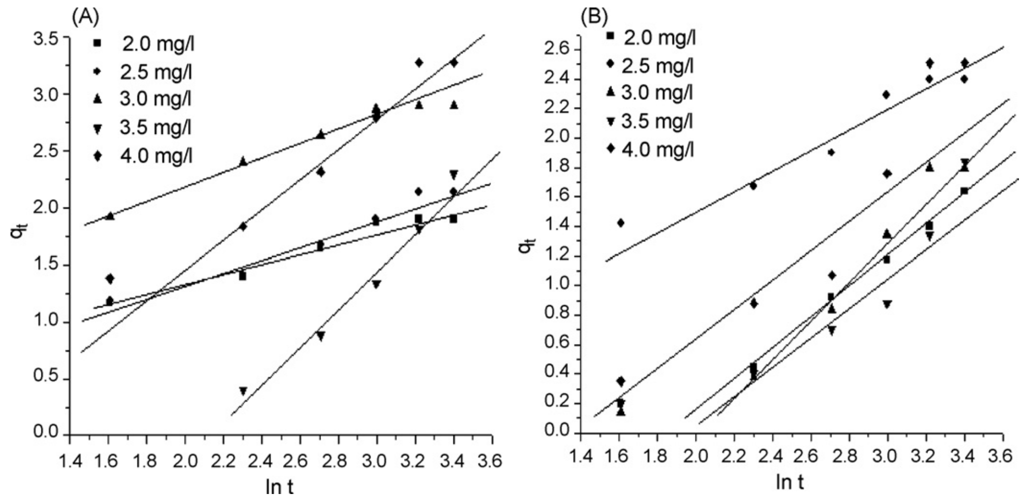

Fig. 10. Elovich model for (A) ATFS and (B) MTFS for various fluoride concentrations.

5.1.1. Langmuir isotherm

The basic Langmuir isotherm model [49], which is based on the monolayer coverage of sorbent surfaces by the sorbate is

$$q_e = \frac{Q^{\circ}bC_e}{1 + bC_e} \quad (5)$$

where q_e and C_e, respectively, are the equilibrium adsorption capacity (mg/g) and the equilibrium adsorbate concentration (mg/l); Q° is the monolayer surface coverage (mg/g) and b is the equilibrium adsorption constant (l/mg).

To evaluate the adsorption capacity and the adsorbate concentration, the aforementioned equation (Eq. (5)) can be used as a linear form as follows:

$$\frac{C_e}{q_e} = \frac{1}{Q^{\circ}b} + \frac{C_e}{Q^{\circ}} \quad (6)$$

The Q° value (i.e., monolayer surface coverage, expressed in units of mg/g) was calculated from the slope of the linear plot of C_e/q_e versus C_e. The related parameters obtained by calculation from the values of the slopes and the intercepts of the respective linear plots are shown in Table 2.

5.1.2. Freundlich isotherm

The basic isotherm model equation developed [50], which is based on the multilayer adsorption of n adsorbate onto the heterogeneous surfaces of an adsorbent, is

$$C_e = K_F C_e^{1/n} \quad (7)$$

where q_e and C_e have the same meaning as noted previously, and K_F and n are empirical constants that are dependent on several environmental factors. The linear form of the Freundlich equation (Eq. (7)), which is commonly used to describe adsorption isotherm data, is

$$\log q_e = \log K_F + \frac{1}{n \log C_e} \quad (8)$$

The plot of $\log q_e$ versus $\log C_e$ of Eq. (8) should result in a straight line. From the slope and the intercept of the plot, the values of n and K_F can be obtained.

5.1.3. Temkin isotherm

The simple form of the Temkin adsorption isotherm model [51], which has been developed considering the chemisorption of the adsorbate onto the adsorbent, is represented as

$$q_e = a + b \log C_e \quad (9)$$

where q_e and C_e have the same meaning as noted previously and the other parameters are called the Temkin constants. The plot of q_e versus $\log C_e$ will generate a straight line. The Temkin constants, a and b, can be calculated from the slope and the intercept of the linear plot of q_e versus $\log C_e$.

The monolayer adsorption capacity (Q°) obtained for ATFS and MTFS was 0.2145 and 0.2178 mg/g, respectively. Thus, it is suggested that the MnO_2-coated TFS has a negligible influence onto fluoride sorption. For both the sorbents, the $1/n$ values came to less then unity, which indicates a favourable sorption, as shown in Table 2.

The Freundlich isotherm model, based on multilayer adsorption, describes the data fairly well (R^2 for ATFS and MTFS = 0.9212 and 0.9396). The Freundlich adsorption constant (K_F) obtained from the linear plot, was 1.58 times greater for MTFS than for ATFS. The Freundlich coefficient (n), which should have values ranging from 1 to 10, was 1.79 times greater for MTFS than for ATFS which supports a favourable sorption of fluoride onto MTFS. The linear plot for Temkin adsorption isotherm, which contains the features of chemisorption, indicated that the sorption of fluoride occurred also by chemical forces.

The present data fit the Langmuir, Freundlich and Temkin isotherm models well, for ATFS, in the following order: Temkin (0.9653) > Langmuir (0.9538) > Freundlich (0.9212) and for MTFS in the following order: Langmuir (0.9538) > Freundlich (0.9396) > Temkin (0.9265).

Another essential feature of the Langmuir model can be projected in terms of a dimensionless separation factor R_L, defined by Weber and Chakravorti [44] as

$$R_L = \frac{1}{1 + bC_o} \quad (10)$$

where C_o and b are the initial fluoride concentration and Langmuir constant, respectively.

The value of R_L indicates the shape of the isotherm to be (i) unfavourable ($R_L > 1$), (ii) linear ($R_L = 1$), (iii) favourable ($0 < R_L < 1$), and (iv) irreversible ($R_L = 0$). In the present work, the R_L values calculated in the studied range of fluoride concentration are determined to be in the range of 0–1, for ATFS and MTFS (R_L value for the fluoride concentration of 2 mg/l is given in Table 2), which suggests the favourable sorption of fluoride onto the studied ATFS and MTFS, under the conditions used for the experiments.

Table 3
Parameters calculated for column experimental data.

Parameters/bed height (cm)	ATFS				MTFS			
	6	9	12	15	6	9	12	15
q_B (mg g^{-1})	0.949	1.103	1.269	1.824	2.564	2.044	1.687	1.525
q_E (mg g^{-1})	0.883	0.941	0.993	0.918	2.688	2.279	1.957	1.986
f	0.140	0.225	0.345	0.380	0.585	0.700	0.770	0.870
h_z	0.206	0.308	0.409	0.511	0.306	0.457	0.607	0.755
k_T (l mg^{-1} min^{-1})	0.349	0.344	0.282	0.244	0.080	0.109	0.079	0.062
q_T (mg g^{-1})	0.365	0.441	1.032	1.420	1.144	1.019	1.226	0.954

6. Column adsorption experiments

ATFS and MTFS are used in the continuous flow column, to investigate the influence of bed depth on the fluoride removal efficiency and to compare the measured adsorption capacities of ATFS and MTFS. For this purpose, columns (0.525 cm^2 of cross-sectional area and 20 cm of height) are packed with 6.798, 10.197, 13.596 and 16.995 g of ATFS and 6.846, 10.269, 13.692 and 17.115 g of MTFS, and used as fixed bed down-flow reactors (6, 9, 12 and 15 cm). The columns were operated using downward flow reactors at 26 ± 1 °C, in the air-conditioned laboratory. The distilled water was run through the columns for 4 h, prior to starting the experiments, in order to wet the column and to establish the equilibrium between the adsorbent and water.

Columns with the bed heights 6, 9, 12 and 15 cm, were used to study the influence of the fluoride adsorption with respect to the increase in bed height. The columns were run using the fluoride solution of 2 mg/l at a pH 6.5.

The capacity at the breakthrough point (q_B) is defined as the amount of fluoride ions bound by ATFS and MTFS, when the concentration of fluoride in the effluent reaches ≈5% of the initial concentration [1]:

$$q_B = \int_0^{V_B} \frac{(C_o - C)}{mdV} \tag{11}$$

where q_B is the capacity at the breakthrough point (mg/g), C_o is the influent fluoride concentration (mg/l), C is the effluent fluoride concentration (mg/l), m is the mass of the sorbent (g), and V_B is the volume of the solution passed up to the breakthrough point (l).

The capacity at the exhaustion point (q_E) corresponds to the amount of the fluoride ions bound by ATFS and MTFS when the concentration of the fluoride in the effluent reaches ≈95% of the initial value [1]:

$$q_E = \int_0^{V_E} \frac{(C_o - C)}{mdV} \tag{12}$$

where q_E is the capacity at the exhaustion point (mg/g), V_E is the volume of solution passed up to the exhaustion point (l), and C_o, C and m have already been defined.

The adsorption columns were operated with different bed depths (6, 9, 12 and 15 cm) until no further fluoride removal was observed. The breakthrough curve for a column is determined by plotting the ratio of the C_e/C_o (C_e and C_o are the fluoride concentrations of effluent and influent, respectively) against the time. A pH deviation of ± 0.15 is observed in the influent water for all columns but the deviations in effluent water, pH up to 0.25 units were observed.

During the process, the influent containing fluoride ions passes through the fixed bed of ATFS and MTFS, and a mass transfer zone, where the fresh solution is in contact with unsaturated ATFS and MTFS, forms [52]. This zone also moves though the column and reaches the exit at the exhaustion point. The height of the mass transfer zone (h_z) can be calculated by the following equation [1]:

$$H_z = \frac{H(HV_E - V_B)}{V_E - (1-f)(V_E - V_B)} \tag{13}$$

where H is the bed depth (cm), f is the parameter which measures the symmetry of the breakthrough curve or the fraction of ATFS or MTFS present in the bed which is still capable of removing the fluoride. The 'f' can be defined as

$$f = \int_0^1 \frac{(1 - C/C_o)d(V - V_B)}{(V_E - V_B)} = \int_{V_B}^{V_E} \frac{(C_o - C)}{C_o(V_E - V_B)dV} \tag{14}$$

where V is the effluent volume (l) and the others are defined as the same as above.

The empty bed contact time (EBCT) or the residence time is usually defined as the relation between the depth of the ATFS and MTFS bed in the column and the influent velocity:

$$\text{EBCT} = \frac{H}{\gamma} \tag{15}$$

where γ is the linear flow rate through the column (cm^3/cm^2/min). The parameters given by Eq. (15) were calculated from the experimental data and are given in Table 3. The increase in bed height increases the empty bed contact time (EBCT) and the height of the mass transfer zone (h_z). The results in Table 3 showed that the breakthrough and the exhaustion capacities were found with negligible changes with respect to the increase in bed height for ATFS and MTFS, which is a main factor for the practical application of this process.

It is too difficult to describe the dynamic behaviour of compound in a fixed bed under defined operating conditions because the process does not occur at a steady state while the influent still passes through the bed. Various simple mathematical models have been developed to describe, and possibly predict, the dynamic behaviour of the bed in column performance [53]. One of these models used for the conditions is the Thomas model [54], which can be written as

$$\frac{C_e}{C_o} = \frac{1}{1 + \exp[k_T(q_T m - C_o V/\theta]} \tag{16}$$

where C_e is the effluent concentration(mg/l), C_o is the influent fluoride concentration (mg/l), k_T is the rate constant (l/mg/min), θ is the flow rate (l/min), q_t is the total sorption capacity (mg/g), V is the throughput volume (l), and m is the mass of the adsorbent.

The linearized form of the Thomas model is as follows:

$$\ln\left[\left(\frac{C_o}{C_e}\right) - 1\right] = \left(\frac{k_T q_T m}{\theta}\right) - \left(\frac{k_T C_o V}{\theta}\right) \tag{17}$$

From the experimental data for C_e, C_o and t at different bed heights, the graphical dependences were plotted in Fig. 11B. The rate constant (k_T) and the total sorption capacity (q_T) can be determined from a plot of $\ln[(C_o/C_e) - 1]$ against time t, for a particular bed height. The model parameters are shown in Table 3.

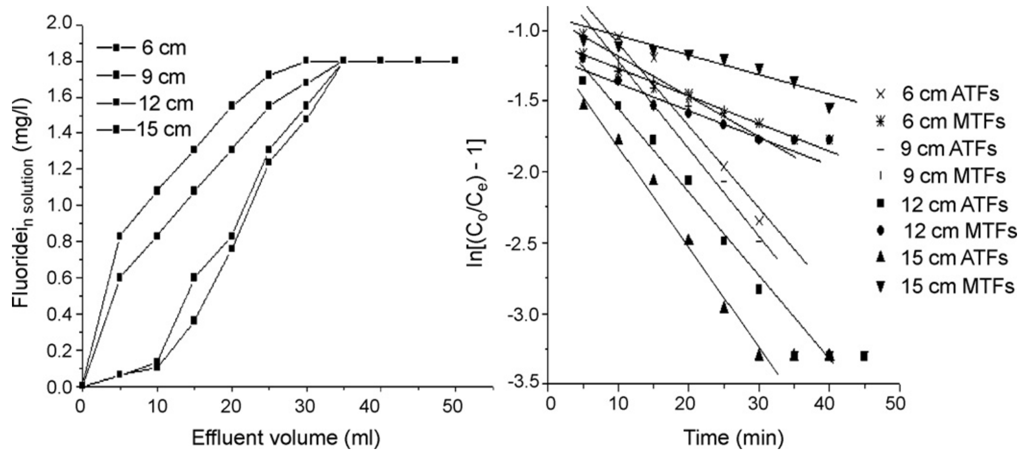

Fig. 11. (A) Breakthrough curve for ATFS and (B) testing of experimental results for ATFS and MTFS by Thomson equation.

In order to provide an adequate test of the Thomas model equation, the total sorption capacity q_T calculated from the Eq. (16) and q_E calculated from the area above the S-curves up to the saturation point, should be close to each other. The agreement of q_T and q_E in Table 3 confirms the applicability of the Thomas model to the examined column system.

The insertion of the calculated parameters k_T and q_T in Eq. (17) for time t, forms the modeled breakthrough curves which are shown (only for ATFS) in Fig. 11A. The satisfactory fitting of the experimental data, modeled through a column of ATFS and MTFS followed the Thomas model. The rate constant, k_T, decreased with respect to the increase in bed height for ATFS, which indicates the increase in the resistance of mass transport. The k_T values of ATFS were greater than those of MTFS and reveal that the mass transport resistance was smaller for ATFS than for MTFS. It was reported [53] that the mass transport resistance is proportional to the axial dispersion and thickness of the liquid film on the particle surface. In the present study, the increase in the bed height increased the mass transport resistance and the axial dispersion, which is confirmed by the decreasing k_T values. The results presented convey that the Thomas equation can be used to predict the breakthrough curves for fluoride removal by a fixed bed of ATFS and MTFS with different bed heights.

7. Conclusion

The present study ascertains the defluoridation potential of activated TFS and manganese oxide-coated TFS. The fluoride removal capacity of the sorbents, ATFS and MTFS, was found to be 1990 mg/kg after the contact time of 30 min, at an optimum pH value of 6.5. The interference of HCO_3^- was observed with a decreased defluoridation percentage of 63.5 and 98 for ATFS and MTFS, respectively. The diffusion-based models revealed that the fluoride sorption onto the above sorbents was governed by the combined effects of the surface and intraparticle diffusion processes. The Freundlich adsorption constant (K_F) of MTFS was found to be 1.58 times greater than that of ATFS. The Temkin isotherm justified the sorption of fluoride which also occurred through chemical forces. From the column experimental results, the fitness of the Thomson equation indicated that the increase in bed height caused an increase in the mass transport resistance and axial dispersion, which was confirmed from the k_T values.

Acknowledgement

The authors thank the Principal and the Management of Thiagarajar College of Engineering (Autonomous), Madurai 625015, Tamil Nadu, India for their support and encouragement.

References

[1] M. Maharamanlioglu, I. Kizilcikli, I.O. Bicer, Adsorption of fluoride from aqueous solution by acid treated spent bleaching earth, J. Fluorine Chem. 115 (2002) 41–47.
[2] T.J. Sorg, Treatment technology to meet the interim primary drinking water regulations for inorganics, J. Am. Water Works Assoc. 70 (1978) 105–111.
[3] A. Sivakamy, K.P. Singh, D. Mohan, M. Maruthamuthu, Studies on defluoridation of water by coal-based sorbents, J. Chem. Tech. Biotech. 76 (2001) 717–722.
[4] Y. Ku, H.M. Chiou, The adsorption of fluoride ion from aqueous solution by activated alumina, Water Air Soil Pollut. 133 (2002) 349–360.
[5] A.K. Chaturvedi, K.P. Yadav, K.C. Pathak, V.N. Singh, Defluoridation of water by adsorption on fly ash, Water Air Soil Pollut. 49 (1990) 51–61.
[6] N. Azbar, A. Turkman, Defluoridation in drinking waters, Water Sci. Technol. 42 (2000) 403–407.
[7] M. Castel, M.O. Schweizer, Simonnot, M. Sardin, Selective removal of fluoride ions by a two-way ion-exchange cyclic process, Chem. Eng. Sci. 55 (2000) 3341–3352.
[8] Z. Amor, B. Barioub, N. Mameri, M. Tuky, S. Nicolas, A. Elmidaoui, Fluoride removal from brackish water by electrodialysis, Desalination 114 (2001).
[9] F. Shen, X.M. Chen, P. Gao, G.H. Chen, Electrochemical removal of fluoride ions from industrial wastewater, Chem. Eng. Sci. 58 (2003) 987–993.
[10] R. Wang, H. Li, Y. Wang, Study of a new adsorbent for fluoride removal from water, Water Qual. Res. J. Can. 30 (1995) 81–88.
[11] D.S. Bhargava, D.J. Killedar, Fluoride adsorption on fishbone charcoal through a moving media adsorber, Water Res. 26 (1992) 781–788.
[12] Y.D. Lai, J.C. Liu, Fluoride removal from water using spent catalyst, Sep. Sci. Technol. 31 (1996) 2791–2797.
[13] S. Mayadevi, Adsorbents for the removal of fluoride from water, Ind. Chem. Eng. A 38 (1996) 155–157.
[14] S.R. Popuri, J. Ajithapriya, N.S.R. Kachireddy, A. Krishnaiah, Biosorption of hexavalent chromium using tamarind (*Tamarindus indica*) fruit shell—a comparative study, Electron. J. Biotech. 10 (2007) 358–367.
[15] D.S. Bharghava, S.B. Sheldarkar, Use of TNSAC in phosphate adsorption studies and relationships. Effects of adsorption operating variables and related relationships, Water Res. 27 (1993) 313–324.
[16] S. Srimachari, Crystalloid interpretation with particular reference to fluoride ion and its possible implications of fluorosis, Arogya 6 (1983) 617–623.
[17] M. Maruthamuthu, J. Venkatanarayanareddy, Binding of fluoride with Tamarind gel, Fluoride 20 (1987) 109–112.
[18] C. Huang, C.P. Huang, Application of *Aspergillus oryzae* and *Rhizopus oryzae* for Cu (II) removal, Water Res. 30 (1996) 1985–1990.
[19] A. Cabuk, S. Ilhan, C. Filik, F. Caliskan, Pb^{2+} biosorption by pretreated fungal biomass, Turk. J. Biol. 29 (2005) 23–28.
[20] S. Venkata Mohan, S.V. Ramanaiah, B. Rajkumar, P.N. Sarma, Removal of fluoride from aqueous phase by biosorption onto algal biosorbent *Spirogyra* sp. IO2: sorption mechanism elucidation, J. Hazard. Mater. 141 (2007) 465–474.
[21] B. Kemer, D. Ozdes, A. Gundogdu, V.N. Bulut, C. Duran, M. Soylak, Removal of fluoride ions from aqueous solution by waste mud from copper mine industry, J. Hazard. Mater. 168 (2009) 888–894.

[22] M. Karthikeyan, K.K. Satheeshkumar, K.P. Elango, Removal of fluoride ions from aqueous solution by conducting polypyrrole, J. Hazard. Mater. 167 (2009) 300–305.
[23] M.S. Onyango, T.Y. Leswifi, A. Ochieng, D. Kuchar, F.O. Otieno, H. Matsuda, Breakthrough analysis for water defluoridation using surface-tailored zeolite in a fixed bed column, Ind. Eng. Chem. Res. 48 (2009) 931–937.
[24] H.X. Wu, T.J. Wang, X.M. Dou, B. Zhao, L. Chen, Y. Jin, Spray coating of adsorbent with polymer latex on sand particles for fluoride removal in drinking water, Ind. Eng. Chem. Res. 47 (2008) 4697–4702.
[25] S. Kagne, S. Jagtap, P. Dhawade, S.P. Kamble, S. Devotta, S.S. Rayalu, Hydrated cement: a promising adsorbent for the removal of fluoride from aqueous solution, J. Hazard. Mater. 154 (2008) 88–95.
[26] A.K. Yadav, C.P. Kaushik, A.K. Haritash, A. Kansal, N. Rani, Defluoridation of groundwater using brick powder as an adsorbent, J. Hazard. Mater. B 128 (2006) 289–293.
[27] W. Ma, F.Q. Ya, M. Han, R. Wang, Characteristics of equilibrium, kinetic studies for adsorption of fluoride on magnetic-chitosan particle, J. Hazard. Mater. 143 (2007) 296–302.
[28] B. Nagappa, G.T. Chandrappa, Mesoporous nanocrystalline magnesium oxide for environmental remediation, J. Hazard. Mater. 106 (2007) 212–218.
[29] L. Lv, Defluoridation of drinking water by calcined Mg–Al–CO_3 layered double hydroxides, Desalination 208 (2007) 125–133.
[30] American Public Health Association (APHA), Standard Methods for the Examination of Water and Wastewater, 21st ed., American Public Health Association (APHA), 1015 Fifteenth Street, NW, Washington DC, 2005.
[31] M.M. Shihabudeen, S. Atul Kumar, L. Philip, Manganese oxide-coated alumina: a promising sorbent for defluoridation of water, Water Res. 40 (2006) 3497–3506.
[32] A. Eskandarpour, M.S. Onyango, A. Ochieng, S. Asai, Removal of fluoride ions from aqueous solution at low pH using Schwertmannite, J. Hazard. Mater. 152 (2008) 571–579.
[33] S. Meenakshi, G. Anitha Pius, B.V. Karthikeyan, Appa Rao, The pH dependence of efficiency of activated alumina in defluoridation of water, Ind. J. Environ. Prot. 11 (1991) 511–513.
[34] R.M. Marathe, U.S. Annapure, R.S. Singhal, P.R. Kulkarni, Gelling behaviour of polyose from tamarind seed kernel polysaccharide, Food Hydrocolloids 16 (2002) 423–426.
[35] R. Yao, F. Meng, L. Zhang, D.D. Ma, M. Wang, Defluoridation of water using neodymium-chitosan, J. Hazard. Mater. 165 (2009) 454–460.
[36] M.S. Onyango, Y. Kojima, O. Aoyi, E.C. Bernardo, M. Matsuda, Adsorption equilibrium modeling and solution chemistry dependence of fluoride removal from water by trivalent-cation-exchanged zeolite, J. Colloid Interface Sci. 279 (2006) 341–350.
[37] M.S. Onyango, Y. Kojima, D. Kuchar, M. Kubota, H. Matsuda, Uptake of fluoride by Al^{3+}-pretreated low-silica synthetic zeolites: adsorption equilibria and rate studies, Sep. Sci. Technol. 41 (2006) 1–22.
[38] S.S. Tripathy, A.M. Raichur, Abatement of fluoride from water using manganese dioxide-coated activated alumina, J. Hazard. Mater. 153 (2008) 1043–1051.
[39] S. Lagergren, Zur theorie der Sogenannten adsorption geloster stoffe, K. Sven. Vetenskapsakad Handl. 24 (1898) 1–39.
[40] C.W. Cheung, J.F. Porter, G. McCay, Sorption kinetic analysis for the removal of cadmium ions from effluents using bone charcoal, Water Res. 35 (2001) 605–612.
[41] M.J.D. Low, Kinetics of chemisorption of gases on solids, Chem. Rev. 60 (1960) 267–312.
[42] S.H. Chien, W.R. Clayton, Application of Elovich equation to the kinetics of phosphate release and sorption in soils, Soil Sci. Soc. Am. J. 44 (1980) 265–268.
[43] D.L. Sparks, in: D.L. Sparks (Ed.), Kinetics of Reactions in Pure and Mixed Systems in Soil Physical Chemistry, CRC Press, Boca Raton, Florida, 1986, pp. 83–145.
[44] T.M. Weber, R.K. Chakravorthi, Pore and solid diffusion models for fixed bed adsorbers, J. Am. Inst. Chem. Eng. 20 (1974) 228–238.
[45] Y.S. Ho, G. McCay, Sorption of dye from aqueous solution by peat, Chem. Eng. J. 70 (1998) 115–127.
[46] N.K. Lazaridis, D.D. Asouhidou, Kinetics of sorptive removal of chromium (VI) from aqueous solution by calcined Mg–Al–CO_3 hydrotalcite, Water Res. 37 (2003) 2875–2882.
[47] S. Venkata Mohan, N. Chandrasekhar Rao, J. Karthikeyan, Adsorption removal of direct azo dye aqueous phase onto coal based sorbents—a kinetic and mechanistic study, J. Hazard. Mater. 90 (2) (2002) 189–204.
[48] S. Sundaram, N. Viswanathan, S. Meenakshi, Defluoridation chemistry of synthetic hydroxyapatite at nanoscale: equilibrium and kinetic studies, J. Hazard. Mater. 155 (2008) 206–215.
[49] I. Langmuir, The constitution and fundamental properties of solids and liquids, J. Am. Chem. Soc. 39 (1916) 2221–2295.
[50] H.M.F. Freundlich, Uber die adsorption in losungen, Z. Phys. chem. 57A (1906) 385–470.
[51] M.J. Temkin, V. Pyzhev, Recent modifications to Langmuir isotherms, Acta Physchim. USSR 12 (1940) 217.
[52] N. Vukojevic, M. Medvidovic, J. Peric, M. Trgo, M.N. Muzek, Removal of lead ions by fixed bed of clinoptilolite—the effect of flow rate, Sep. Purif. Technol. 49 (2006) 298–304.
[53] Z. Aksu, F. Gonen, Biosorption of phenol by immobilized activated sludge in a continuous packed bed: Prediction of breakthrough curves, Process Biochem. 39 (2004) 599–613.
[54] H.C. Thomas, Heterogeneous ion exchange in a flowing system, J. Am. Chem. Soc. 66 (1944) 1664–1666.